Original Research Article

Genome Mining of Siderophore-Producing *Streptomyces* sp. from the *Melissa officinalis* Rhizosphere

Audrey Farrell[1], Robert Samples[2], Riccardo Racicot[2], and Lesley-Ann Giddings[1, 2]

[1]*Department of Chemistry, Smith College, 100 Green Street, Northampton, MA 01063, United States;*
[2]*Biochemistry Program, Smith College, 100 Green Street, Northampton, MA 01063, United States*

ABSTRACT

Siderophores, iron-chelating secondary metabolites, are crucial to plant growth and commonly produced by organisms in the rhizosphere. These specialized molecules have found applications across a wide range of industries, such as medicine and bioremediation. Members of the *Lamiaceae* family are environmentally beneficial for phytoremediation, the removal of heavy metals from soil, as chelated metals do not impact essential oil production. Herein, we used culture-based screening, genome sequencing, and LC-MS/MS metabolomics to recover and characterize a siderophore-producing bacterial isolate from the rhizosphere of *Melissa officinalis*, a medicinal member of the *Lamiaceae* family not previously studied in this context, and to evaluate cerium-associated changes in its metabolomic profile as an initial, exploratory step toward assessing its relevance to bioremediation. Using a Chrome Azurol S (CAS) assay, we isolated siderophore-producing bacteria. Genomic sequencing revealed that an isolate was *Streptomyces* sp. (AF-1A) with a genome size of 7.9 Mbp and 71.96% GC content. antiSMASH analysis revealed three siderophore biosynthetic gene clusters, one of which corresponded to the known cluster for desferrioxamines B and E. Several siderophores, including desferrioxamines B, E, D_1, and G_1, desoxynocardamine, and desmethylenylnocardamine, were putatively identified using LC-MS/MS. The latter four show a statistically significant increase in relative abundance in the presence of the rare earth element cerium; the remaining two (desferrioxamines B and E) were present at levels too low for quantitative comparison and were identified from MS/MS fragmentation alone. Nearly 40% of *Streptomyces* sp. AF-1A molecular features were exclusive to the rare earth element cerium conditions, suggesting this strain has a strong response in siderophore biosynthesis to lanthanide elicitation. AF-1A shows a metabolomic response to environmental levels of cerium, warranting further investigation as a candidate for siderophore-based bioremediation strategies, pending direct tests of metal tolerance, chelation efficiency, and process-scale feasibility.

Keywords: *Melissa officinalis*; *Streptomyces*; genomics; siderophore biosynthesis; metabolomics; Chrome Azurol S

Corresponding author: Lesley-Ann Giddings, E-mail: lgiddings@smith.edu.

Accepted September 3, 2026
https://doi.org/10.70251/HYJR2348.45214225

INTRODUCTION

Siderophores are low-molecular-weight iron-chelating agents produced by bacteria, fungi, and plants to assist in iron uptake (1, 2). Although iron is the fourth most abundant element in the Earth's crust, it is often inaccessible to plants and microbes because its solubility

is dependent on its oxidation state (3). Ferrous iron (Fe^{2+}) is more water-soluble than ferric iron (Fe^{3+}), but under the aerobic, neutral-to-alkaline conditions typical of most soils, iron is thermodynamically favored in the ferric state, which rapidly precipitates as insoluble oxides and hydroxides and is therefore poorly bioavailable (4). Ferric iron is involved in essential metabolic processes, such as the electron transport chain, biosynthesis of chlorophyll, and repair of DNA, but is scarcely found in the rhizosphere due to its insolubility at neutral pH (4). Thus, rhizosphere microorganisms produce siderophores to scavenge for ferric iron, assisting plants with nutrient acquisition (5).

Although the primary function of siderophores is to increase ferric iron bioavailability, these molecules have been shown to bind to other metals and metalloids, such as copper, nickel, zinc, and cerium (6, 7). This diverse metal-binding ability enables siderophores to have many industrial applications in medicine and agriculture (2). Within agricultural contexts, siderophores are useful in bioremediation and phytoremediation, using microbes or plant siderophores, respectively, to remove metals from environments contaminated by pesticides, fertilizers, and improper industrial waste disposal (8). These are economically and environmentally favorable alternatives to conventional soil heavy metal remediation involving the excavation or landfilling of metal-polluted soils (2,9). These unique metabolites also show promise in the bioremediation of rare-earth metals or lanthanide pollution, which is increasing due to their growing use in technology, making the discovery of novel siderophores and the biosynthetic gene clusters that produce them an important and exciting field of research (6, 7).

Several studies on siderophores and their biosynthetic gene clusters have focused on rhizosphere actinobacteria due to their well-documented siderophore-producing abilities, assisting plants with nutrient acquisition (10). The rhizospheres of plants in the family *Lamiaceae* have been reported to contain siderophore-producing actinobacteria (11). However, no known studies have focused on *Melissa officinalis*, a medicinal herb native to the Mediterranean region (11, 12) (Figure 1). *M. officinalis*, commonly known as lemon balm, is also of interest because of its extensive medicinal properties, such as antioxidant, anti-inflammatory, and antimicrobial activity (13). Furthermore, members of the *Lamiaceae* family are effective in phytoremediation, the removal of heavy metals from soils, without impacting essential oil production, making the rhizosphere of *M. officinalis* an environmentally beneficial sampling site for the isolation and identification of iron-chelating siderophores and their producers (13, 14). Herein, we hypothesized that siderophore-producing actinobacteria can be isolated from the rhizosphere of *M. officinalis* to be sequenced and analyzed for siderophore biosynthetic gene clusters (BGCs).

Figure 1. *Photograph of Melissa officinalis, the plant from which rhizosphere soil and roots were sampled.*

This study aimed to identify a siderophore-producing bacterial isolate from the *M. officinalis* rhizosphere using colorimetric Chrome Azurol S (CAS) overlay assays, genomic sequencing, and metabolomics. Given the increasing presence of naturally occurring rare earth metals due to anthropogenic inputs (e.g., mining) and their reported modulation of secondary metabolism, microbial cultures were supplemented with cerium to determine its effects on rhizosphere microbial siderophore production (2, 11, 14). Such integration of multi-omics and elicitation approaches provides a case study for screening metal-responsive siderophore producers for bioremediation of metal-polluted environments.

METHODS AND MATERIALS

Sample Collection and Preparation

M. officinalis roots and rhizosphere soil were collected in a sterile manner from the Lyman Conservatory at Smith College in Northampton, MA, in September 2024. A single sample of soil and roots collected from one plant (Accession number 2003-0173) was baked in the oven at 50 °C for one hour and twenty minutes, respectively, to select for sporulating bacteria. Soil (0.5007 g dry mass)

was diluted in 5.0 mL of autoclaved water. Roots (0.20 g dry mass) were sanitized with 70% ethanol and ground with 4 mL of autoclaved water using a mortar and pestle. Samples were plated on GYM agar plates [glucose (4 g/L), yeast extract (2 g/L), malt extract (2 g/L), Difco agar (BD Biosciences; Franklin Lake, New Jersey) (20 g/L), nalidixic acid (20 mg/L), and cycloheximide (80 mg/L)]. Soil and root mixtures were shaken for one hour at room temperature. Dilutions (10^0–10^{-2}) were subsequently made and centrifuged at 6000 x *g* for 3 minutes before the supernatant (100 µL) was plated on GYM agar and incubated at 37 °C for seven days. Colonies were subsequently streaked onto GYM plates without antibiotic and antifungal agents (nalidixic acid and cycloheximide) and incubated at 37 °C for 2 days for future DNA extraction. Three isolates were selected on the basis of morphological characteristics, with Actinomycetota being targeted for their high biosynthetic capacity.

CAS Overlay, Antibacterial, and Antifungal Assays

CAS overlay assays of the isolates were prepared according to Louden B.C. et al (2011). Glassware was acid-washed with 6 M HCl and rinsed with ddH_2O to remove trace iron. A blue dye solution was prepared by combining CAS (60 mg in 50 mL ddH_2O), $FeCl_3{\cdot}6H_2O$ (2.7 mg in 10 mL of 10 mM HCl), and hexadecyltrimethylammonium bromide (HDTMA; 73 mg in 40 mL ddH_2O). Separately, an agar base was mixed using MM9 salts (15 g/L KH_2PO_4, 25 g/L NaCl, 50 g/L NH_4Cl), 32.24 g/L PIPES buffer (adjusted to pH 6.8 with NaOH), and 15 g/L Bacto agar, autoclaved, and cooled to 50 °C. Iron-free casamino acids (3 g) and 20% (w/v) glucose were added to the cooled agar base, followed by the blue dye solution, which was added slowly along the vessel wall with agitation to ensure thorough mixing before plates were poured (15).

After pouring the CAS overlays, plates were incubated at room temperature for 48 hours (18). Antibacterial and antifungal assays were conducted by spreading *Bacillus subtilis*, *Aspergillus flavus*, and *A. niger* on the entirety of a GYM plate without antimicrobial agents. Isolates were spotted in the center of each quadrant on each plate, which were then incubated at 37 °C for one week. Two isolates with larger (>5 mm) zones of CAS-positive reaction were selected for sequencing.

DNA extraction, Library Preparation, and Sequencing

The ZymoBIOMICs DNA microprep kit (Zymo Research; Irvine, CA) was used to extract genomic DNA from colonies of isolate 1A. The quality and size distribution of the samples were analyzed via Agilent Fragment Analyzer 5200 (Agilent; Santa Clara, CA), and the DNA concentration was determined via Qubit 4 Fluorometer (Thermo Fisher Scientific; Waltham, MA). DNA was then prepared for sequencing through the NEBNext UltraExpress FS Library Prep Kit (New England BioLabs; Ipswich, MA). Paired-end libraries (2 x 151 bp) were prepared using MiSeq Reagent Kit V3 (600 cycles) (Illumina; San Diego, CA). Sequencing was performed on an Illumina MiSeq at the Center for Molecular Biology at Smith College (Northampton, MA). *Streptomyces* sp. AF-1A was selected for further analysis on the basis of having lower assembly fragmentation.

De Novo Genome Assembly and Analysis

The raw sequence reads of isolate AF-1A were uploaded to the Galaxy (www.usegalaxy.org) platform version 24.1, accessed November 2024, where all pre-annotation analysis was conducted (16). Concatenate datasets tail-to-head tool (1.0.0) was used to combine the raw data from each run (17). Trimmomatic (version 0.39+galaxy2) was used to remove low-quality reads and adapter sequences (18). FastQC (version 0.12.1) was then used to examine the quality of the raw reads (19). Next, de novo assembly was performed with Unicycler (version 21.20.50), and the assembled genome was evaluated using the Quality Assessment Tool for Genome Assemblies (QUAST version 21.46.33) (assembly statistics reported here reflect QUAST's default 500 bp minimum contig length threshold; 456 raw Unicycler contigs were reduced to 401 after this filter) (20,21). Assembly completeness was assessed by BUSCO (version 6.1.0) using the actinomycetes_odb12 dataset (22). Next, the NCBI BLAST + blastn tool [NCBI NT (01 Sept 2023)] (version 2.14.1+galaxy2) was used for taxonomic identification (23) by comparing the whole genome against the NCBI Whole-Genome Shotgun contigs database. Taxonomic identification was further assessed using the Type (Strain) Genome Server (TYGS) (24). Furthermore, Sanger sequencing of the bacterial 16S rRNA gene using 27F and 1492R primers further confirmed the taxonomic identification (25). Prokka (version 1.14.6+galaxy2) (26) was then used to annotate the genome, followed by antiSMASH (version 6.1.1), a bioinformatics tool used to annotate secondary metabolite biosynthetic gene clusters (27). The genome was also uploaded to the Rapid Annotation using Subsystem Technology (RAST) platform accessed on 10 December 2024 for visualization with the SEED viewer (version 2.0) (28).

Liquid Chromatography-Mass Spectrometry Metabolomics Studies

GYM liquid media (5 mL) was inoculated with AF-1A spores, vortexed, and the OD_{600} was adjusted to 0.08-0.12. Cultures were prepared in 96-well plates in triplicate in the following manner and incubated without shaking at 30 °C for 7 days: control cultures consisted of 180 µL of GYM liquid media and 20 µL inoculant; Ce-elicited cultures 160 µL GYM liquid media, 20 µL prepared inoculant, and 20 µL of 2.5 mM sodium cerium edetate stock solution (to promote secondary metabolite production); and a sterility blank with 200 µL GYM liquid media. Edetate growth controls were not included, as free EDTA would perturb free metal balance, nor were sodium cerium edetate sterility controls. After culturing, 200 µL from each well was added to 200 µL of LC-MS grade methanol, mixed, sonicated for 60 seconds, and centrifuged for 5 minutes at 6000 x *g* before LC-MS analysis.

A Thermo Scientific (Waltham, MA) Q-exactive HF-X Hybrid Quadrupole-Orbitrap mass spectrometer interfaced with a Vanquish Horizon Ultra high-performance liquid chromatography (UHPLC) system and VH-D10-A UV detector using a Waters (Milford, MA) HSS T3 C18 column (1.8 µm, 2.1 × 150 mm) was used for analysis. Using a flow rate of 0.5 mL $minute^{-1}$, samples (2 µL) were injected onto the column. The column chamber temperature was maintained at 40 °C. UHPLC separation was achieved using the following gradient method: 2% acetonitrile: 98% water with 0.1% formic acid for 1 min, 2–40% over 4 min, 40–98% over 3 min, 98–2% over 0.2 min, and 2% for 2 min. The UV-Vis data were collected with 200-300, 300-400, 400-500, and 500-600 nm channels. The following electrospray ionization (ESI) settings were used in probe position D: 40 sheath gas flow, 8 auxiliary gas flow, 1 sweep gas flow, 3.5 kV spray voltage, 380 °C capillary temperature, 50 radiofrequency (RF) funnel level, and 350 °C auxiliary gas temperature. A Top 5 data-dependent acquisition (DDA) method was used with MS1 (60,000 resolution) and MS2 (15,000 resolution) scans between 150-2,000 *m/z*.

Raw data were processed in MS-DIAL v5.5.241113 (29) with default settings using the following modifications: profile data for MS1 and MS2, [M+H] and [M+Na] adducts selected, a minimum peak-picking threshold of $3e^5$, an MS2 annotation intensity cutoff of 1% with 4 minimum matched peaks to the MS-DIAL ESI(+)-MS/MS database from authentic standards. A single injection of one of the 250 µM Ce-treated cultures was used as an alignment reference with an alignment window of 0.2 minutes. As the total injection volume was effectively normalized to a set volume of the original fermentation broth, no further normalization steps were applied to the data. The resulting peak lists were analyzed with MPACT v1.00 r24.11.17 (30). Data were filtered and visualized using the following settings: median coefficient of variation filter threshold of 0.2 across technical triplicates, a solvent blank group filtering and group parsing threshold of 0.01 relative abundance, and both raw in-source filtering and mispicked peak filters were disabled. In this hierarchical design (n = 3 technical replicates, n = 3 well replicates), MPACT assumes technical and well replicate uncertainties are uncorrelated and estimates effective degrees of freedom using the Welch–Satterthwaite equation; the resultant v_{eff} and σ are used to perform Welch's t-test with Benjamini-Hochberg FDR correction ($q < 0.05$) for the generation of volcano plots. Herein, we use MPACT's terminology for denoting levels in the hierarchical replication model; the biological replicate level consists of well replicates, and the technical replicate level consists of repeated injections from each extracted well. Targeted analysis was performed using Thermo Freestyle 1.8 SP2. All annotations were confirmed to match NIST 23 (similarity reported by EI hybrid similarity score) and/or MS-DIAL reference spectral libraries (29,31).

Data Sharing and Nucleotide Accession Numbers

Genome assembly and metadata were submitted to the National Center for Biotechnology Information under BioProject identifier PRJNA1212225. The 16S ribosomal RNA gene sequence used for analyses was deposited in Figshare (https://doi.org/10.6084/m9.figshare.29333030).

RESULTS AND DISCUSSION

The rhizosphere is an environment in which nutrients, including metal cations, are exchanged, pre-selecting for siderophore-producing bacteria (2). Based on the growing interest in the bioremediation of metal-polluted environments, the goal of this study was to isolate siderophore-producing actinobacteria from the *M. officinalis* rhizosphere and evaluate their siderophore production under various conditions through genomic and metabolomic analyses. By combining genomic and metabolomic methods, we aimed to understand siderophore biosynthetic pathways in *M. officinalis* rhizosphere bacteria and the effect of metals, such as rare earth metals, on siderophore production to better understand their use in bioremediation.

Isolation and Characterization of AF-1A

The initial cultivation of the *M. officinalis* rhizosphere soil and root samples yielded a wide array of bacterial and fungal colonies. Colonies were selected for isolation based on their actinobacterial morphology. Isolate AF-1A was selected for further analysis based on its morphology, siderophore production, and antifungal activity. When cultivated on GYM media with nalidixic acid and cycloheximide, isolate AF-1A was observed to be small, round, entire, flat, grey, and dry in its morphology (Figures 2A–B). AF-1A produced a diffusible brown pigment that was most prominent in areas of medium-density colonies, suggesting it may be regulated by a quorum-sensing or autoregulator-controlled biosynthetic pathway (32,33). CAS overlay assays confirmed that AF-1A exhibited the greatest siderophore activity among the isolates, as indicated by an orange halo (i.e., CAS-positive region) extending more than 5 mm beyond the colony (Figure 2c). It is also notable that CAS reactivity was strongest in regions where colonies were present at high densities on the T-streak plate, similar to the production distribution of the aforementioned diffusible brown pigment, potentially suggesting similar regulatory control of siderophore production (32,33). This heterogeneous response complicated quantitative evaluation of CAS halo diameter. While antibacterial and antifungal assays revealed AF-1A did not demonstrate antibacterial activity against *B. subtilis* or *A. flavus,* AF-1A did demonstrate minor antifungal activity against *A. niger*, as evidenced by the small zone of inhibition surrounding it on the assay plate (Figure 2d).

De Novo Genome Assembly and Analysis

Isolate AF-1A was sequenced to identify its taxonomy and siderophore-producing gene clusters. The draft genome assembly for AF-1A comprised 401 contigs totaling 7,908,993 bp, with the largest contig of 262,095 bp, N50 of 34,933 bp (L50 = 59), and N90 of 9,605 bp (L90 = 222). The assembly contained no ambiguous bases and had an average GC content of 71.96% and a completeness of 95.8%. Genome annotation with Prokka predicted 7,139 coding sequences, 84 tRNAs, 5 rRNAs, 2 repeat regions, and 1 tmRNA. The total number of reads was 1,733,554, and 1,704,483 reads passed quality control, corresponding to an estimated mean sequencing depth of ~65x. A comparison of the 16S ribosomal RNA gene and draft genome to the NCBI database confirmed that AF-1A was a *Streptomyces* sp., with the top BLASTn hit for the largest assembled contig (262,095 bp) showing 92.7% nucleotide identity over a 10,318 bp alignment to GenBank WGS accession AYRX01000082.1, *Streptomyces* sp. GXT6. RAST annotation of this genome revealed several genes involved in iron acquisition and metabolism as well as secondary metabolism (Figure 3). Genome BLAST Distance Phylogeny (GBDP) analysis of the whole genome placed AF-1A in a clade with type strains *S. puniciscabiei* DSM 41929, *S. barringtoniae* JA03, and *S. durhamensis* NRRL B-3309.

Genes involved in secondary metabolism were further explored via antiSMASH analyses, which revealed that the draft genome of AF-1A contained three biosynthetic gene clusters involved in siderophore biosynthesis (Table 1). Of these three biosynthetic gene clusters, two produced unknown products, and one was 100% identical to genes involved in the biosynthesis of the siderophore desferrioxamine B/E. These data demonstrate the potential of this bacterium to produce new siderophores, especially as one gene cluster does not resemble any other known siderophore biosynthetic gene cluster. However, low or negligible antiSMASH

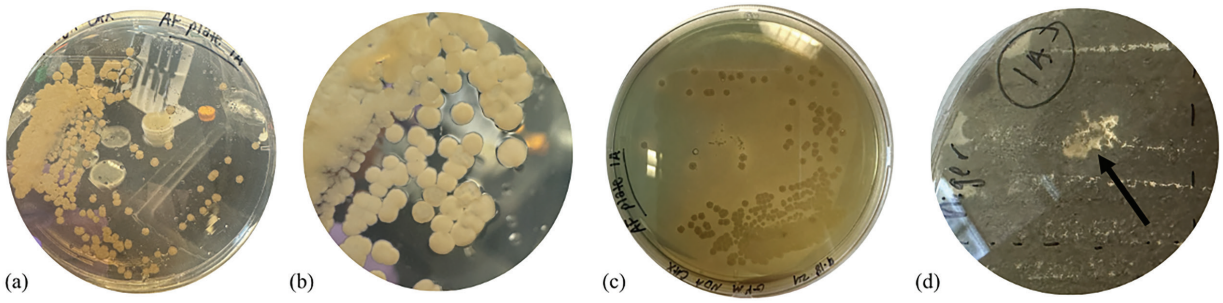

Figure 2. *Images of isolate AF-1A: (a) GYM agar with nalidixic acid and cycloheximide (b) close-up of colonies on GYM agar with nalidixic acid and cycloheximide (c) CAS overlay assay (d) antifungal assay with A. niger on GYM agar. The black arrow indicates a small zone of inhibition.*

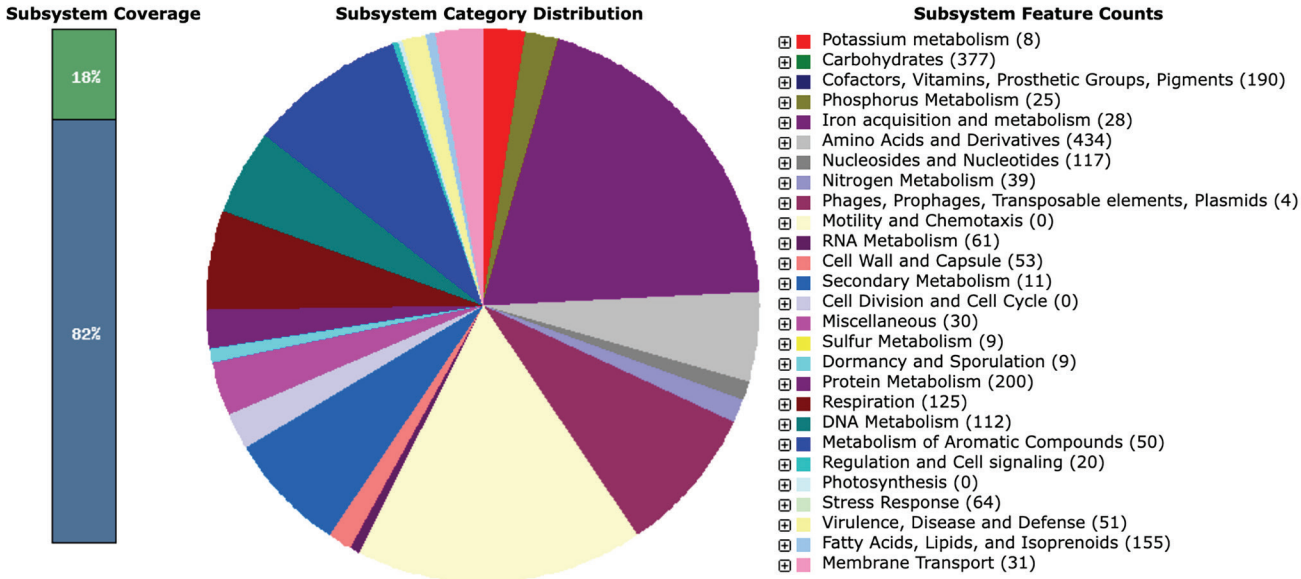

Figure 3. *Subsystem category distribution of Streptomyces sp. AF-1A genome visualized with the SEED viewer (version 2.0) from RAST (29).*

Table 1. *Putative gene clusters in the predicted genome of Streptomyces sp. AF-1A.*

Type	Region Number	Beginning-End	Cluster Lengths (bp)	Most Similar Known Cluster	Similarity
siderophore	21.1	34,698-64,467	29,769	Desferrioxamine B/E	100%
siderophore	24.1	8,497-39,620	31,123	Nonribosomal peptide-independent siderophore	8%
siderophore	36.1	30,589-47,561	16,972	Nonribosomal peptide-independent siderophore	0%

similarity scores do not, by themselves, establish that these clusters produce structurally novel compounds, and the presence of a desferrioxamine-like cluster does not confirm that every hydroxamate-type metabolite detected by LC-MS/MS originates from that specific cluster; establishing these links directly would require targeted gene knockouts or heterologous expression (34).

Liquid Chromatography-Mass Spectrometry Analysis

LC-MS/MS analyses identified siderophores produced by *Streptomyces* sp. AF-1A under different growth conditions, including the presence of high concentrations of the rare earth element cerium to observe its effects on siderophore production. This lanthanide is environmentally relevant as it is one of the most abundant rare earth elements in the Earth's crust and is commonly added to fertilizer as a biostimulant, increasing its concentration in soil over time (35). Importantly, cerium has been shown to impact *Streptomyces* secondary metabolism as well as increase siderophore production in other bacteria (14, 36). The UpSet plot in Figure 4 shows the features after MPACT filtering procedures by biological group presence/absence, with a sizable proportion of the features not present in media controls detected only in the presence of cerium, in comparison to those produced in both cerium and control conditions. Approximately 40% (104 of 259 microbial features) of features not found in the sterility control are exclusive to the cerium conditions, demonstrating that *Streptomyces* sp. AF-1A fermentation broth displays a greater number of features not present in the media control under lanthanide elicitation conditions.

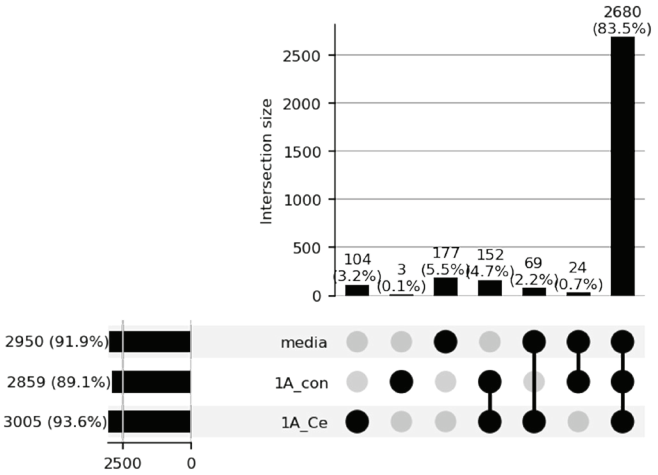

Figure 4. *UpSet plot showing the percentage of spectral features unique to growth conditions, media = media blank, 1A_con = AF-1A, and 1A_Ce = AF-1A treated with 250 μM cerium. Of the microbial features that were not present in the sterility control, most (104 of 259) were only detected in the presence of cerium. Only three features were unique to the control culture, and 152 features were present in both culture conditions.*

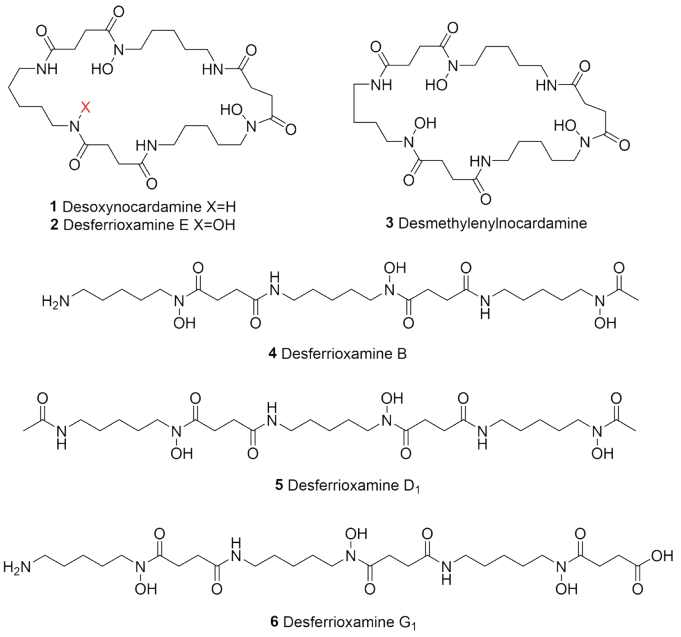

Figure 5. *Structures of siderophores observed via LC-MS from cultures of Streptomyces sp. AF-1A.*

LC-MS/MS analysis putatively annotated several siderophores produced by *Streptomyces* sp. AF-1A, including the cyclic hydroxamates desoxynocardamine, desferrioxamine E, and desmethylenylnocardamine (**1–3**), as well as the linear desferrioxamines B, D_1, and G_1, (**4–6**, Figure 5, Table 2). Due to the oligomeric nature of desferrioxamines, fragmentation patterns across the class are highly similar and automatic annotation based solely on fragmentation, as is the case with the National Institute of Standards and Technology (NIST) database, frequently returns highly matches for other members of the family. Thus, the automated NIST match for these features (Table 2) must be interpreted as a class annotation. For each putative annotation at least seven diagnostic fragments were present for the hydroxamate siderophore class, and High Resolution Mass Spectrometry (HRMS) identification at sub 3 ppm mass error for the parent ion precludes assignment of alternative formulae for compounds in this class. For desferrioxamine B specifically automated annotation using NIST did not return a hydroxamate as a match and thus none is reported in Table 2, this is due to the low abundance of this compound and presence of coeluting compounds within the isolation window resulting in chimeric spectra, nonetheless the parent ion was detected with 2.85 ppm error (HRMS (ESI+) *m/z*: $[M+H]^+$ 561.3606 calcd for $C_{25}H_{49}N_6O_8^+$; found, 561.3622), and seven class diagnostic fragments were detected for succinyl cadaverine-type hydroxamate siderophores (Table 2). These annotations correspond to Level 2 putative compound annotations on common untargeted metabolomics confidence frameworks (37).

In addition to detection of these putative hydroxamate siderophores in targeted analysis, the volcano plot in Figure 6 demonstrates that compounds **1**, **3**, **5**, and **6** were also identified using untargeted metabolomics, and that cerium treatment induced a statistically significant increase in the accumulation of these four compounds. Desferrioxamines E (**2**) and B (**4**) were present at intensities too low to pass MPACT's automated feature-detection filtering and were instead putatively annotated from their MS/MS fragmentation patterns alone. Consequently, their relative abundance was not quantitatively compared between conditions, and they are not shown in Figure 6. Notably, compounds **3** and **6** were unique to cerium-treated cultures. Thus, the addition of cerium could be used to increase structural diversity and quantity of hydroxamate siderophores produced, including clinically relevant compounds such as desferrioxamine B (**4**) (38).

The cerium-associated shift in the AF-1A metabolomic profile is consistent with a growing body of evidence that rare earth elements act as chemical elicitors

Table 2. *Table of putatively annotated hydroxamate siderophores. Note that an automatic library match was not obtained for the feature putatively annotated as desferrioxamine E due to coeluting compounds of similar mass resulting in a chimeric spectra.*

Compound	Formula	t_R (min)	Theoretical [M+H]	Experimental *m/z*	PPM Error	NIST Library Match (Score)	Diagnostic Fragments (*m/z*)
Deoxynocardamine (**1**)	$C_{27}H_{48}N_6O_8$	4.59	585.3606	585.3614	1.37	Terragine E (823)	84, 86, 100, 102, 140, 168, 185, 201 257, 267, 285, 319, 385
Desferrioxamine E (**2**)	$C_{27}H_{48}N_6O_9$	4.75	601.3556	601.356	0.7	Nocardamine (838)	56, 70, 84, 100, 102, 112, 122, 138, 154, 165, 183, 201, 219, 283
Desmethylenyl-nocardamine (**3**)	$C_{26}H_{46}N_6O_9$	4.53	587.3399	587.3411	2.0	Terragine E (586)	56, 70 84, 86, 100, 102, 112, 138, 140
Desferrioxamine B (**4**)	$C_{25}H_{48}N_6O_8$	3.71	561.3606	561.3622	2.85		56, 84, 86, 70, 86 201, 219
Desferrioxamine D_1 (**5**)	$C_{27}H_{50}N_6O_9$	3.85	603.3712	603.372	1.3	Terragine E (735)	84, 86, 100 102, 165, 168, 185, 201, 267, 385
Desferrioxamine G_1 (**6**)	$C_{27}H_{50}N_6O_{10}$	3.937	619.3661	619.3668	1.13	Nocardamine (602)	84, 86, 100 102, 165, 184, 201, 283

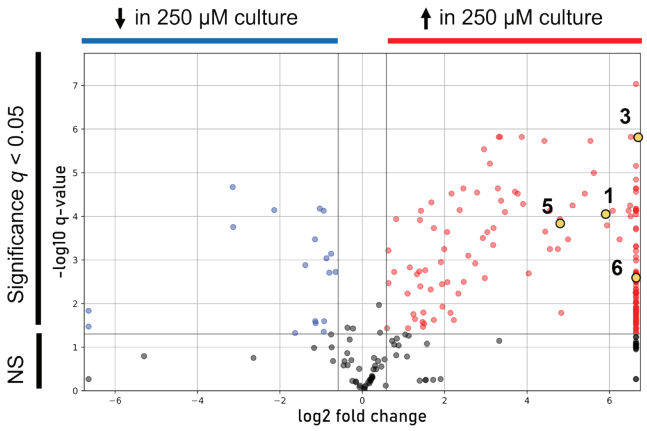

Figure 6. *Volcano plot showing the statistically significant change in LC-MS/MS peak intensity of features putatively annotated as desoxynocardamine (1), desmethylenylnocardamine (3), desferrioxamine D_1 (5), and desferrioxamine G_1 (6) in AF-1A cultures treated with cerium edetate versus untreated controls (n = 3 technical replicates, n = 3 well replicates, and Welch's t-test with Benjamini-Hochberg FDR correction, q < 0.05).*

of cryptic or under-expressed secondary metabolism in *Streptomyces* (14). Tanaka et al. (2010) showed that low concentrations of scandium and lanthanum activated nine secondary metabolite biosynthetic gene clusters in *S. coelicolor* A3(2) by 2.5- to 12-fold and revealed metabolites detectable only in rare-earth-treated cultures. This pattern is broadly analogous to the cerium-exclusive molecular features observed here, though the present study extends this elicitor effect specifically to cerium and to a desferrioxamine-type hydroxamate siderophore cluster. This finding also complements related work from our group on *Streptomyces* sp. PD-S100-1 (39) and *Streptomyces* sp. ADLamb9 (40), isolated from the rhizospheres of *Cyperus virens* and *Lavandula dentata* (also a *Lamiaceae* species), respectively, in which cerium exposure differentially altered the accumulation of catecholate and hydroxamate siderophores (40), and on *Streptomyces* sp. PTY087I2, in which cerium exposure revealed previously undetected thiolated metabolites (30). Together, these studies suggest that rare-earth-induced metabolomic shifts may be a broader feature of rhizosphere-associated *Streptomyces* rather than isolate-specific. The capacity of lanthanides to modulate bacterial gene expression more generally is also supported by work in methanotrophs, where cerium regulates methanol dehydrogenase expression independent of siderophore biosynthesis (14, 36), underscoring that its effects on secondary metabolism likely operate through more than one, still only partly understood, mechanism.

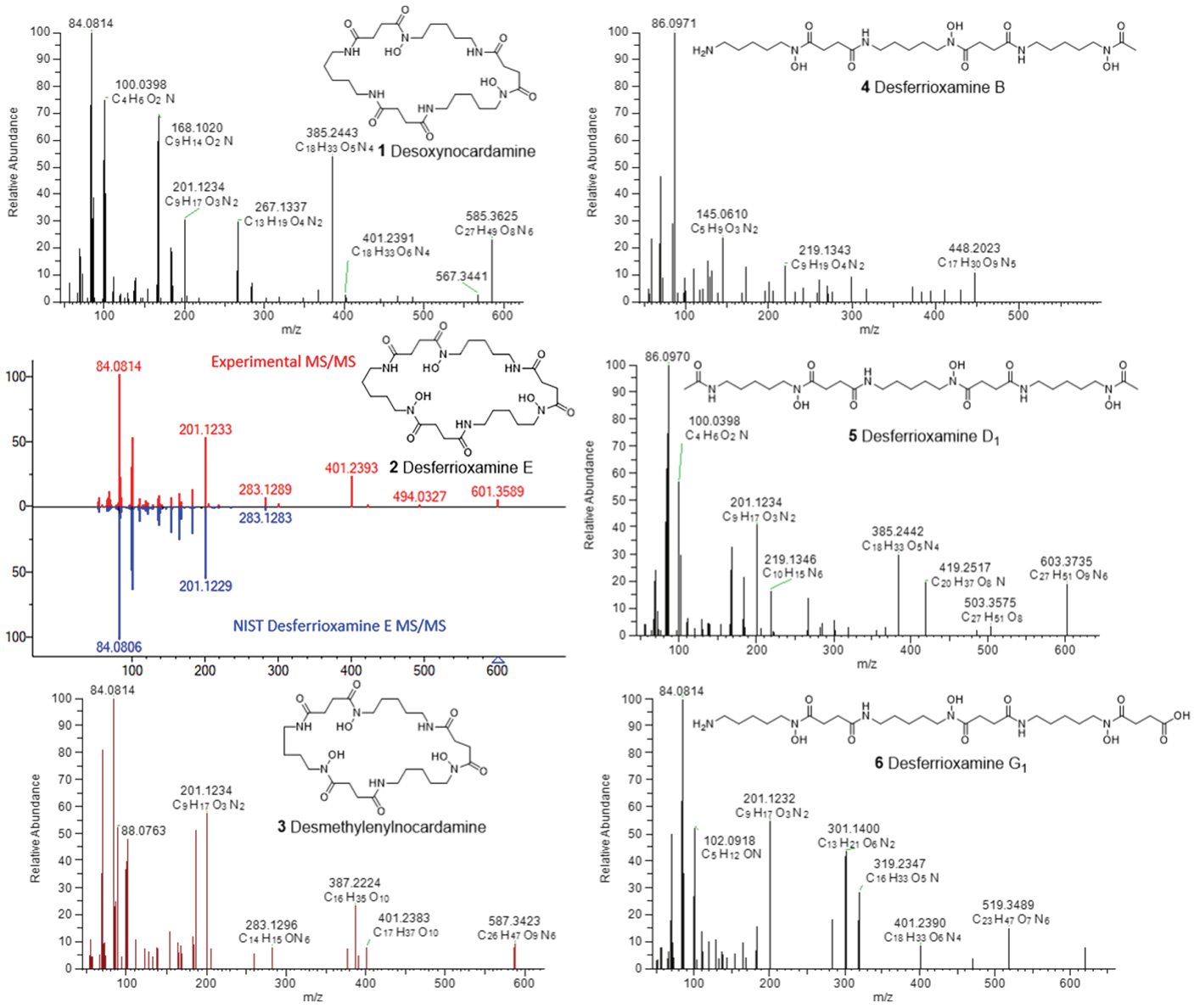

Figure 7. *Experimental MS/MS fragmentation patterns for putatively annotated compounds 1-6, with a mirror plot of experimental MS/MS (red) for desferrioxamine E (2) and a NIST 23 database fragmentation pattern for the same compound (blue).*

Several limitations qualify these findings. The genome assembly remains fragmented (401 contigs), which can affect the completeness and resolution of biosynthetic gene cluster boundaries. LC-MS/MS compound assignments are putative and should be treated as tentative pending orthogonal confirmation with authentic standards. Metabolomic comparisons were relative rather than absolute, and matched edetate-only controls were not included, so effects specific to cerium cannot be fully distinguished from effects of the edetate chelator itself. However, due to the high stability constant of cerium edetate (LogK ≈ 16.0), the complex is highly unlikely to dissociate, and as such, free edetate in media or cultures is a poor control, as free EDTA would bind essential metals in a way cerium edetate does not (41). Additionally, previous studies have generally not included a discrete lanthanide-treated sterility control (14, 30, 42). While we have provided statistical measures

of increases in levels of putatively annotated compounds, it is not possible to give absolute quantification in terms of concentration. However, in untargeted metabolomics studies relative abundance is commonly used given standards may not be available for all compounds detected (37, 43-45). Finally, the bioremediation relevance discussed here is exploratory and would need to be confirmed through dedicated metal-chelation and growth-tolerance assays.

CONCLUSION

Selecting siderophore-producing actinobacteria from the rhizosphere of *M. officinalis* using CAS overlay assays successfully led to the isolation of *Streptomyces* sp. AF-1A. Genomic analyses supported the siderophore-producing potential of *Streptomyces* sp. AF-1A by detecting three siderophore biosynthetic gene clusters, two of which did not match any known cluster and remain uncharacterized. One of these clusters closely matched the known biosynthetic pathway for desferrioxamines, putatively annotated forms of which were observed through LC-MS/MS analysis. Desoxynocardamine (**1**), desmethylenylnocardamine (**3**), and desferrioxamines D_1 (**5**) and G_1 (**6**) showed a statistically significant increase in relative abundance in the presence of cerium. Together, these genomic and metabolomic data identify *Streptomyces* sp. AF-1A as a promising candidate for further study of cerium-responsive siderophore biosynthesis and, pending direct tests of metal tolerance and chelation efficiency, a candidate worth evaluating for bioremediation applications in cerium-containing environments.

ACKNOWLEDGEMENTS

We gratefully recognize Smith College Lyman Plant House and Conservatory (Jimmy Grogan), Smith College Center for Molecular Biology, and Smith College Center for Mass Spectrometry.

FUNDING SOURCES

This work was supported by the Faculty Early Career Development (CAREER) Award from the National Science Foundation (NSF) (grant number 2236643 for A. F., R. S., R. R., and L-A. G.). We also thank the Department of Chemistry at Smith College for supporting this work.

CONFLICT OF INTEREST

The authors declare that there are no conflicts of interest related to this work.

REFERENCES

1. Kurth C, Kage H, Nett M. Siderophores as molecular tools in medical and environmental applications. *Org Biomol Chem*. 2016; 14 (35): 8212–27. doi:10.1039/C6OB01400C
2. Knapp M, Giddings LA. Bacterial Siderophore Production in Metal-Rich Environments: Underexplored Sources of Siderophores and Insights into Bioremediation. *J Nat Prod*. 89 (3): 846–63. doi:10.1021/acs.jnatprod.5c01586
3. Kumar M, Poonam, Ahmad S, Singh RP. Plant growth promoting microbes: Diverse roles for sustainable and ecofriendly agriculture. *Energy Nexus*. 2022 Sep 1; 7: 100133. doi:10.1016/j.nexus.2022.100133
4. Vijay K, Shibasini M, Sivasakthivelan P, Kavitha T. Microbial siderophores as molecular shuttles for metal cations: sources, sinks and application perspectives. *Arch Microbiol*. 2023 Aug 29; 205 (9): 322. doi:10.1007/s00203-023-03644-3 PubMed PMID: 37644212.
5. Ahmed E, Holmström SJM. Siderophores in environmental research: roles and applications. *Microb Biotechnol*. 2014 Feb 27; 7 (3): 196–208. doi:https://doi.org/10.1111/1751-7915.12117
6. Kotelnikova AD, Rogova OB, Stolbova VV. Lanthanides in the Soil: Routes of Entry, Content, Effect on Plants, and Genotoxicity (a Review). *Eurasian Soil Sci*. 2021 Jan 1; 54 (1): 117–34. doi:10.1134/S1064229321010051
7. Roskova Z, Skarohlid R, McGachy L. Siderophores: an alternative bioremediation strategy? *Sci Total Environ*. 2022 May 1; 819: 153144. doi:10.1016/j.scitotenv.2022.153144
8. Briffa J, Sinagra E, Blundell R. Heavy metal pollution in the environment and their toxicological effects on humans. *Heliyon*. 2020 Sep 1; 6 (9): e04691. doi:10.1016/j.heliyon.2020.e04691
9. Gomes AFR, Almeida MC, Sousa E, Resende DISP. Siderophores and metallophores: Metal complexation weapons to fight environmental pollution. *Sci Total Environ*. 2024 Jul 1; 932: 173044. doi:10.1016/j.scitotenv.2024.173044
10. Alexander DB, Zuberer DA. Use of chrome azurol S reagents to evaluate siderophore production by rhizosphere bacteria. *Biol Fertil Soils*. 1991 Sep 1; 12 (1): 39–45. doi:10.1007/BF00369386

11. Mohamad OAA, Liu YH, Huang Y, Li L, Ma JB, Egamberdieva D, et al. The Metabolic Potential of Endophytic Actinobacteria Associated with Medicinal Plant Thymus roseus as a Plant-Growth Stimulator. *Microorganisms*. 2022 Sep; 10 (9): 9. doi:10.3390/microorganisms10091802
12. Shirokikh IG, Mokrushina SE. Streptomycetes from the Rhizosphere of Three Medicinal Plants as Plant Growth Stimulants and Biocontrol Agents. *Mosc Univ Biol Sci Bull*. 2024 Jun 1; 79 (2): 78–85. doi:10.3103/S0096392524600881
13. Carvalho F, Duarte AP, Ferreira S. Antimicrobial activity of *Melissa officinalis* and its potential use in food preservation. Food Biosci. 2021 Dec 1;44:101437. doi:10.1016/j.fbio.2021.101437
14. Tanaka Y, Hosaka T, Ochi K. Rare earth elements activate the secondary metabolite–biosynthetic gene clusters in Streptomyces coelicolor A3(2). *J Antibiot (Tokyo)*. 2010 Aug; 63 (8): 477–81. doi:10.1038/ja.2010.53
15. Louden BC, Haarmann D, Lynne AM. Use of Blue Agar CAS Assay for Siderophore Detection. J Microbiol Biol Educ. 2011. Located at: world. doi:10.1128/jmbe.v12i1.249
16. Goecks J, Nekrutenko A, Taylor J, The Galaxy Team. Galaxy: a comprehensive approach for supporting accessible, reproducible, and transparent computational research in the life sciences. *Genome Biol*. 2010 Aug 25; 11 (8): R86. doi:10.1186/gb-2010-11-8-r86
17. Blankenberg D, Von Kuster G, Bouvier E, Baker D. Dissemination of scientific software with Galaxy ToolShed. *Genome Biol*. 2014; 15 (403). doi:https://doi.org/10.1186/gb4161
18. Bolger AM, Lohse M, Usadel B. Trimmomatic: a flexible trimmer for Illumina sequence data. *Bioinformatics*. 2014 Aug 1; 30 (15): 2114–20. doi:10.1093/bioinformatics/btu170
19. Andrews S. Babraham Bioinformatics [Internet]. [cited 2025 Mar 7]. FastQC A Quality Control tool for High Throughput Sequence Data. Available from: https://www.bioinformatics.babraham.ac.uk/projects/fastqc/
20. Molina-Mora JA, Campos-Sánchez R, Rodríguez C, Shi L, García F. High quality 3C de novo assembly and annotation of a multidrug resistant ST-111 Pseudomonas aeruginosa genome: Benchmark of hybrid and non-hybrid assemblers. *Sci Rep*. 2020 Jan 29; 10 (1): 1392. doi:10.1038/s41598-020-58319-6
21. Mikheenko A, Valin G, Prjibelski A, Saveliev V, Gurevich A. Icarus: visualizer for de novo assembly evaluation. *Bioinformatics*. 2016 Nov 1; 32 (21): 3321–3. doi:10.1093/bioinformatics/btw379
22. Simão FA, Waterhouse RM, Ioannidis P, Kriventseva EV, Zdobnov EM. BUSCO: assessing genome assembly and annotation completeness with single-copy orthologs. *Bioinformatics*. 2015 Oct 1; 31 (19): 3210–2. doi:10.1093/bioinformatics/btv351 PubMed PMID: 26059717.
23. Camacho C, Coulouris G, Avagyan V, Ma N, Papadopoulos J, Bealer K, et al. BLAST+: architecture and applications. *BMC Bioinformatics*. 2009 Dec 15; 10 (1): 421. doi:10.1186/1471-2105-10-421
24. Meier-Kolthoff JP, Göker M. TYGS is an automated high-throughput platform for state-of-the-art genome-based taxonomy. Nat Commun. 2019 May 16; 10 (1): 2182. doi:10.1038/s41467-019-10210-3
25. Frank JA, Reich CI, Sharma S, Weisbaum JS, Wilson BA, Olsen GJ. Critical Evaluation of Two Primers Commonly Used for Amplification of Bacterial 16S rRNA Genes. *Appl Environ Microbiol*. 2008 Apr 15; 74 (8): 2461–70. doi:10.1128/AEM.02272-07
26. Seemann T. Prokka: rapid prokaryotic genome annotation. *Bioinformatics*. 2014 Jul 15; 30 (14): 2068–9. doi:10.1093/bioinformatics/btu153
27. Blin K, Shaw S, Kloosterman AM, Charlop-Powers Z, van Wezel GP, Medema MH, et al. antiSMASH 6.0: improving cluster detection and comparison capabilities. *Nucleic Acids Res*. 2021 Jul 2; 49 (W1): W29–35. doi:10.1093/nar/gkab335
28. Aziz RK, Bartels D, Best AA, DeJongh M, Disz T, Edwards RA, et al. The RAST Server: Rapid Annotations using Subsystems Technology. *BMC Genomics*. 2008 Feb 8; 9 (1): 75. doi:10.1186/1471-2164-9-75
29. Tsugawa H, Cajka T, Kind T, Ma Y, Higgins B, Ikeda K, et al. MS-DIAL: data-independent MS/MS deconvolution for comprehensive metabolome analysis. *Nat Methods*. 2015 Jun; 12 (6): 523–6. doi:10.1038/nmeth.3393
30. Samples RM, Puckett SP, Balunas MJ. Metabolomics Peak Analysis Computational Tool (MPACT): An Advanced Informatics Tool for Metabolomics and Data Visualization of Molecules from Complex Biological Samples. *Anal Chem*. 2023 Jun 13; 95 (23): 8770–9. doi:10.1021/acs.analchem.2c04632
31. Wang M, Carver JJ, Phelan VV, Sanchez LM, Garg N, Peng Y, et al. Sharing and community curation of mass spectrometry data with Global Natural Products Social Molecular Networking. *Nat Biotechnol*. 2016 Aug 9; 34 (8): 828–37. doi:10.1038/nbt.3597 PubMed PMID: 27504778; PubMed Central PMCID: PMC5321674.
32. Horinouchi S. A microbial hormone, A-factor, as a master switch for morphological differentiation and secondary metabolism in Streptomyces griseus. *Front Biosci J Virtual Libr*. 2002 Oct 1; 7: d2045-2057. doi:10.2741/A897 PubMed PMID: 12165483.

33. Liu G, Chater KF, Chandra G, Niu G, Tan H. Molecular Regulation of Antibiotic Biosynthesis in Streptomyces. *Microbiol Mol Biol Rev MMBR*. 2013 Mar; 77 (1): 112–43. doi:10.1128/MMBR.00054-12 PubMed PMID: 23471619; PubMed Central PMCID: PMC3591988.
34. Matine I, Clasen F, Guevara FG, Guo M, Shoaie S. Regulatory and metabolic control of microbial biosynthetic gene clusters. *Commun Biol*. 2026 Jul 17; 9 (1): 982. doi:10.1038/s42003-026-10623-z
35. Moreira CG, Carvalho TS de, de Oliveira C, Abreu LB de, Castro ACS de, Ribeiro PG, et al. Ecological risk assessment of cerium for tropical agroecosystems. *Chemosphere*. 2019 Apr 1; 221: 124–31. doi:10.1016/j.chemosphere.2018.12.195
36. Gu W, Semrau JD. Copper and cerium-regulated gene expression in Methylosinus trichosporium OB3b. *Appl Microbiol Biotechnol*. 2017 Dec 1; 101 (23): 8499–516. doi:10.1007/s00253-017-8572-2
37. Alseekh S, Aharoni A, Brotman Y, Contrepois K, D'Auria J, Ewald J, et al. Mass spectrometry-based metabolomics: a guide for annotation, quantification and best reporting practices. *Nat Methods*. 2021 Jul; 18 (7): 747–56. doi:10.1038/s41592-021-01197-1 PubMed PMID: 34239102; PubMed Central PMCID: PMC8592384.
38. Bellotti D, Remelli M. Deferoxamine B: A Natural, Excellent and Versatile Metal Chelator. *Molecules*. 2021 May 28; 26 (11): 3255. doi:10.3390/molecules26113255 PubMed PMID: 34071479; PubMed Central PMCID: PMC8198152.
39. Dennison P, Samples R, Racicot R, Giddings LA. Siderophore Production by a Rhizosphere-Associated Streptomyces from Cyperus virens. *Am J Undergrad Res*. 2026 Jan; 22 (4). doi:10.33697/ajur.2025.158
40. Dely A, Racicot R, Samples R, Giddings LA. Draft genome sequence and metabolomics data for Streptomyces sp. ADLamb9 isolated from the rhizosphere of Lavandula dentata. *Data Brief*. 2025 Oct 24; 63: 112199. doi:10.1016/j.dib.2025.112199 PubMed PMID: 41278148; PubMed Central PMCID: PMC12630106.
41. Smith RM, Martell AE. Critical stability constants, enthalpies and entropies for the formation of metal complexes of aminopolycarboxylic acids and carboxylic acids. *Sci Total Environ*. 1987 Jun 1; Environmental Inorganic Chemistry 64 (1): 125–47. doi:10.1016/0048-9697(87)90127-6
42. Kawai K, Wang G, Okamoto S, Ochi K. The rare earth, scandium, causes antibiotic overproduction in Streptomyces spp. *FEMS Microbiol Lett*. 2007 Sep; 274 (2): 311–5. doi:10.1111/j.1574-6968.2007.00846.x PubMed PMID: 17645525.
43. Zytnick AM, Gutenthaler-Tietze SM, Aron AT, Reitz ZL, Phi MT, Good NM, et al. Identification and characterization of a small-molecule metallophore involved in lanthanide metabolism. *Proc Natl Acad Sci*. 2024 Aug 6; 121 (32): e2322096121. doi:10.1073/pnas.2322096121
44. Goodwin CR, Covington BC, Derewacz DK, McNees CR, Wikswo JP, McLean JA, et al. Structuring microbial metabolic responses to multiplexed stimuli via self-organizing metabolomics maps. *Chem Biol*. 2015 May 21; 22 (5): 661–70. doi:10.1016/j.chembiol.2015.03.020 PubMed PMID: 25937311; PubMed Central PMCID: PMC4537791.
45. Lee JY, Han Y, Styczynski MP. Towards inferring absolute concentrations from relative abundance in time-course GC-MS metabolomics data. *Mol Omics*. 2023 Feb 20; 19 (2): 126–36. doi:10.1039/d2mo00168c PubMed PMID: 36374123; PubMed Central PMCID: PMC9974747.